Dalton Transactions

PAPER

View Article Online
View Journal | View Issue

Cite this: *Dalton Trans.*, 2019, **48**, 15657

New examples of triangular terbium(III) and holmium(III) and hexagonal dysprosium(III) single molecule toroics†‡

Stuart K. Langley,*[a] Kuduva R. Vignesh,[b] Tulika Gupta,[b] Christopher J. Gartshore,[c] Gopalan Rajaraman,*[b] Craig M. Forsyth[c] and Keith S. Murray*[c]

Received 7th June 2019,
Accepted 27th August 2019

DOI: 10.1039/c9dt02419k

rsc.li/dalton

The structural, magnetic and theoretical aspects are described for three triangular lanthanide complexes, $[Tb^{III}_3(OH)(teaH_2)_3(paa)_3]Cl_2$ (**1**), $[Dy^{III}_3(OH)(teaH_2)_3(paa)_3]Cl_2$ (**2**) and $[Ho^{III}_3(OH)(teaH_2)_3(paa)_3]Cl_2$ (**3**), and a hexanuclear wheel of formula $[Dy^{III}_6(pdeaH)_6(NO_3)_6]$ (**4**) [$teaH_3$ = triethanolamine, paaH = *N*-(2-pyridyl)-acetoacetamide and $pdeaH_3$ = 3-[bis(2-hydroxyethyl)amino]propan-1-ol]. Each complex displays single molecule toroidal behaviour as rationalised using high-level *ab initio* calculations. Complexes **2** and **3** are the first examples of mixed moment single molecule toroidal complexes featuring non-Kramers ions.

Introduction

Since the pioneering work by Powell *et al.*[1] on toroidal dysprosium(III) triangular complexes, the field of single molecule toroics (SMTs) has grown rapidly from both experimental and theoretical viewpoints.[1,2] Some highlights include the discovery of toroidal magnetism in planar rings such as $\{Dy_4\}$[3] and $\{Dy_6\}$,[4] non-planar (cubanoid) $\{Dy_4\}$[5] and mixed d–f-block species such as $\{Cu^{II}Dy_3\}$ chains,[6] large $\{Cu^{II}_6Dy_6\}$ rings,[7] and 'double triangular' $\{Dy_3Cr^{III}Dy_3\}$ heptanuclear clusters,[8] the last example showing the rare phenomenon of ferrotoroidal behaviour. Toroidal moments are reported mainly for Dy^{III} complexes,[9] however, we have recently reported SMTs containing Tb^{III} and Ho^{III} ions.[4b,10] The growth in the subject is not only because of the fundamental knowledge to be gained about SMTs but also because of the possible applications in areas such as quantum information processing,[11] high-density data storage and as nanoscale devices such as molecular spin valves and spin transistors.[11a,12] Molecular based devices offer the advantage of tuneable properties, whereby the electronic structure of the molecule can be influenced by the coordination environment of the lanthanide ion, which can be exploited to modify the physical properties.

One of the chemico-structural design problems in SMT chemistry is to design ligand and bridging moieties, in lanthanide ring complexes, that will lead unambiguously to toroidal behaviour, proven by magnetic and computational data. In the present work we describe the structures and magnetism of three triangular complexes, $[Tb^{III}_3(OH)(teaH_2)_3(paa)_3]Cl_2{\cdot}MeCN{\cdot}4H_2O$ (**1**), $[Dy^{III}_3(OH)(teaH_2)_3(paa)_3]Cl_2{\cdot}MeCN{\cdot}4H_2O$ (**2**) and $[Ho^{III}_3(OH)(teaH_2)_3(paa)_3]Cl_2{\cdot}MeCN{\cdot}4H_2O$ (**3**), and a new hexagonal 6-ring compound $[Dy^{III}_6(pdeaH)_6(NO_3)_6]{\cdot}6H_2O$ (**4**) [$teaH_3$ = triethanolamine, paaH = *N*-(2-pyridyl)-acetoacetamide and $pdeaH_3$ = 3-[bis(2-hydroxyethyl)amino]propan-1-ol (Fig. 1)]. The synthesis, structure and preliminary magnetism have been reported for **2**.[13] We show *via* a combination of experimental and theoretical *ab initio* calculations that each complex display a rotating magnetic moment in the exchange coupled ground magnetic state, thus revealing SMT behaviour.

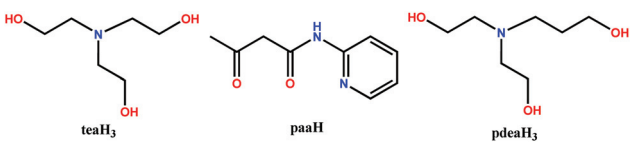

Fig. 1 Molecular structure of ligands – $teaH_3$, paaH and $pdeaH_3$.

[a]*School of science and the environment, Division of Chemistry, Manchester Metropolitan University, Manchester, M15 6BH, UK. E-mail: s.langley@mmu.ac.uk*
[b]*Department of Chemistry, Indian Institute of Technology Bombay, Mumbai-400076, India. E-mail: rajaraman@chem.iitb.ac.in*
[c]*School of Chemistry, Monash University, Clayton, Victoria 3800, Australia. E-mail: keith.murray@monash.edu*

†Dedicated to Professor Annie K. Powell on the celebration of her 60th birthday and for her contributions to molecular magnetism and inorganic chemistry.

‡Electronic supplementary information (ESI) available: Additional molecular structures, structural parameter tables, magnetic plots and calculated values. CCDC numbers 1915658 (**1**), 1940155 (**2**), 1915657 (**3**) and 1915659 (**4**). For ESI and crystallographic data in CIF or other electronic format see DOI: 10.1039/c9dt02419k

Experimental section

General information

The reactions were carried out under aerobic conditions. Chemicals and solvents were obtained from commercial sources and used without further purification.

Synthesis of $[Tb^{III}_3(OH)(teaH_2)_3(paa)_3]Cl_2{\cdot}MeCN{\cdot}4H_2O$ (1). $TbCl_3{\cdot}6H_2O$ (0.38 g, 1.0 mmol) was used following the method reported for **2**.[13] Within 1–2 days block-shaped crystals of **1** had formed, in approximate yield of 57%. Anal. calc. for **1**: $Tb_3C_{47}H_{81}O_{20}N_{10}Cl_2$: C, 34.13; H, 4.94; N, 8.47. Found: C, 34.24; H, 4.99; N, 8.63%.

Synthesis of $[Dy^{III}_3(OH)(teaH_2)_3(paa)_3]Cl_2{\cdot}MeCN{\cdot}4H_2O$ (2).[13] The synthesis for **1** was followed with $DyCl_3{\cdot}6H_2O$ (1 mmol) used in place of $TbCl_3{\cdot}6H_2O$ and has been described previously.[13] Within 1–2 days block-shaped crystals of **2** had formed, in approximate yield of 63%. Anal. calc. for **2**: $Dy_3C_{47}H_{81}O_{20}N_{10}Cl_2$: C, 33.91; H, 4.90; N, 8.41. Found: C, 33.60; H, 4.87; N, 8.31%.

Synthesis of $[Ho^{III}_3(OH)(teaH_2)_3(paa)_3]Cl_2{\cdot}MeCN{\cdot}4H_2O$ (3). The synthesis for **1** was followed with $HoCl_3{\cdot}6H_2O$ (1 mmol) used in place of $TbCl_3{\cdot}6H_2O$. Within 1–2 days block-shaped crystals of **3** had formed, in approximate yield of 63%. Anal. calc. for **3**: $Ho_3C_{47}H_{81}O_{20}N_{10}Cl_2$: C, 33.76; H, 4.88; N, 8.38. Found: C, 33.87; H, 4.76; N, 8.56%.

Synthesis of 3-[bis(2-hydroxyethyl)amino]propan-1-ol ($pdeaH_3$). Diethanolamine (5.25 g, 53 mmol), 3-chloropropanol (5.0 g, 53 mmol) and KOH (3.0 g, 53 mmol were refluxed in H_2O (25 ml) for 12 hours. After this time the reaction was cooled and the solid filtered. The solid was rinsed with a minimal amount of cold EtOH and the solvent was evaporated. The product was obtained as a viscous yellow oil.

Synthesis of $[Dy^{III}_6(pdeaH)_6(NO_3)_6]{\cdot}6H_2O$ (4). $Dy(NO_3)_3{\cdot}6H_2O$ (0.44 g, 1.0 mmol) was dissolved in $MeOH/CH_2Cl_2$ (1 : 3, 20 mL), followed by the addition of 3-[bis(2-hydroxyethyl)amino]propan-1-ol (0.13 mL, 1.0 mmol) and triethylamine (0.55 mL, 4.0 mmol) which resulted in a colourless solution. This was stirred for 6 hours, after which the solution was filtered to remove any precipitate and layered with diethylether (Et_2O). Within 1–2 days block-shaped crystals of **4** had formed, in approximate yield of 23%. Anal. calc. for **4**: $Dy_6C_{42}H_{102}O_{42}N_{12}$: C, 20.85; H, 4.24; N, 6.94. Found: C, 21.21; H, 4.45; N, 7.32%.

X-ray crystallography

X-ray measurements for **1–4** were performed at 123 K using a Bruker Smart Apex X8 diffractometer using Mo K_α radiation. The structure of **2** has been reported previously.[13] The data collection and integration were performed within SMART and SAINT+ software programs and corrected for absorption using the Bruker SADABS program. Compounds **1–4** were solved by direct methods (SHELXS-97),[14] and refined (SHELXL-2018/3)[15] by full matrix least-squares on all F^2 data.[16] Crystallographic data and refinement parameters are summarized in Table S1.‡ Crystallographic details are available in the ESI‡ in CIF format. CCDC numbers 1915658 (**1**), 1940155 (**2**), 1915657 (**3**) and 1915659 (**4**).‡

Magnetic measurements

The magnetic susceptibility measurements were carried out on a Quantum Design SQUID magnetometer MPMS-XL 7 operating between 1.8 and 300 K for dc-applied fields ranging from 0–5 T. Microcrystalline samples were dispersed in Vaseline in order to avoid torquing of the crystallites. The sample mulls were contained in a calibrated gelatine capsule held at the centre of a drinking straw that was fixed at the end of the sample rod. Alternating current (ac) susceptibility measurements were carried out under an oscillating ac field of 3.5 Oe and frequencies ranging from 0.1 to 1500 Hz.

Computational details

The magnetic properties of all the Ln^{III} centres in complexes **1–4** were studied by fragment *ab initio* calculations using MOLCAS 8.0[17] following methods described recently for Ln^{III}_6 wheel species.[4b] Accounting for the role imposed by neighbouring metal centres, for **1–3**, and using fragmented calculation, one Ln^{III} ion of interest was kept intact, while the other two sites were substituted by diamagnetic La^{III} ions.[18,19] (see ESI‡ for more information about computational details of complexes **1–3**).[20] In **4**, as in our earlier study,[4b] we fragmented the $\{Dy_6\}$ wheel into a trinuclear species and have substituted neighbouring ions with a diamagnetic Lu^{III} ion. The model fragment is shown in Fig. S1 of ESI.‡ The computed SO states have been incorporated into the SINGLE_ANISO[21] program to compute the *g*-tensors. Crystal-field parameters were obtained using the SINGLE_ANISO code.

The exchange/dipolar interactions between neighbouring Ln^{III}–Ln^{III} ions of **1–4** have been computed by fitting with the experimental magnetic data[4c,6,22] using the Lines model[23] within the POLY_ANISO routine.[24] The exchange Hamiltonian employed for complexes **1–4** is shown in eqn (1).

$$\hat{H}_{ex} = -\sum_{i=1}^{3} J_i \cdot S_i \cdot S_{i+1} \quad (1)$$

(here $J_i = J_i^{dipolar} + J_i^{exch}$; *i.e.* J_i are the total magnetic interaction of the calculated $J_i^{dipolar}$ and fitted J_i^{exch} parameters; this describes the interaction between all the neighbouring metal centres).

Results and discussion

Triangular compounds **1–3** (Fig. 2) are isomorphous and the structure of **2** has been described earlier.[13] The three Ln^{III} ions are all eight coordinate with triangular dodecahedron geometries with the deviation of 1.38 (Table S2‡) as predicted by SHAPE software.[25] The molecules pack in a way that large channels are observable, which are filled with the disordered solvent water and MeCN molecules (Fig. S2‡). Selected bond lengths for **1–3** are given in Table S3.‡

Compound **4** crystallizes in the trigonal space group, $R\bar{3}$, with the asymmetric unit containing one Dy^{III} ion. It contains six Dy^{III} ions, with a planar wheel metallic core structure

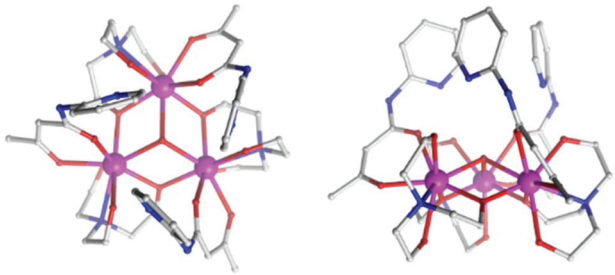

Fig. 2 Molecular structure of **1**, (left) top view, (right) side view. Colour scheme Tb^{III}, pink; O, red; N, blue; C, grey, the H-atoms and chloride counter ions are omitted for clarity. The same structure is applicable for **2** and **3**.

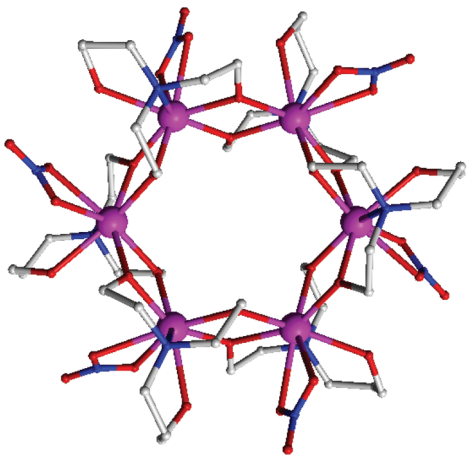

Fig. 3 Molecular structure of **4**. Colour scheme Dy^{III}, pink; O, red; N, blue; C, grey, the H-atoms are omitted for clarity.

(Fig. 3) similar to analogues we described earlier.[4b] The Dy^{III} ions are eight coordinate with triangular dodecahedron geometries with the deviations of 2.24 as predicted by SHAPE software (Table S2‡).[25] Selected bond lengths and angles for **4** are shown in Table S3.‡

We note that the metal topology and first coordination sphere is identical to a previously reported $\{Dy_6\}$ wheel.[4b,c] : The key structural difference is the protonated alcohol arm, which constitutes the 3-carbon alcohol arm chain (a 2-carbon chain in previous complexes), which chelates to the Dy^{III} site that is bonded to the N-atom. It has been shown that changing the coordinating atom, bond length and bond angle can have a big effect on the magnetic behaviour of lanthanide complexes.[26] In previous works we revealed that the $\{Dy_6\}$ wheel displays a toroidal magnetic moment in the ground state.[4b,c] Powell and co-workers subsequently reported how ligand field variations affected the toroidal behaviour in two other related $\{Dy_6\}$ wheels.[4a] Due to the inclusion of the extra $-CH_2-$ arm we find subtle structural modifications compared to the parent $\{Dy_6\}$ wheel which we envisage will influence the toroidal and dynamic relaxation behaviour. We find that average Dy···Dy bond length and Dy–O–Dy angles are 3.73 Å and 110.5°, respectively for **4** compared to 3.73 Å and 110.1° of the parent $\{Dy_6\}$ wheel. See Table S4‡ for a comparison of $Dy–L_{N/O}$ bond lengths, which are significantly different.[4b]

Magnetic properties

Magnetic susceptibility data were collected on polycrystalline samples of **1–4** between 2 and 300 K. DC fields of 1 T and 0.1 T (Fig. S3 in ESI‡) were employed and, since the results were similar, the data for the 1 T field are shown in Fig. 4, plotted as $\chi_M T$ *versus* T. The experimental magnetic data of **2** is retained from ref. 13 for comparing it with the *ab initio* calculated data in this work. The room temperature values of 35.46, 41.63 (ref. 13) and 41.39 cm^3 K mol^{-1} for **1–3**, respectively, agree well with the calculated values of 35.61, 42.51 and 42.21 cm^3 K mol^{-1}. The $\chi_M T$ values decrease gradually down to 20 K, before a sharper drop occurs below this temperature, reaching values of 8.66, 16.72 and 11.73 cm^3 K mol^{-1} at 2 K. The decrease is due to the depopulation of the crystal field split Stark sublevels of the appropriate ground state, with possible weak antiferromagnetic exchange and/or dipolar interactions also contributing to the behaviour (see Theoretical analysis). The magnetization values in the M *versus* H plots {shown in Fig. 4 and Fig. S4–S6‡} do not saturate indicating the presence of anisotropy and/or weak magnetic interactions, with values of magnetization at 5 T and 2 K of 15.26, 17.03 and 19.52 $N\mu_B$ for **1–3**, respectively. Interestingly, for **1**, we observe

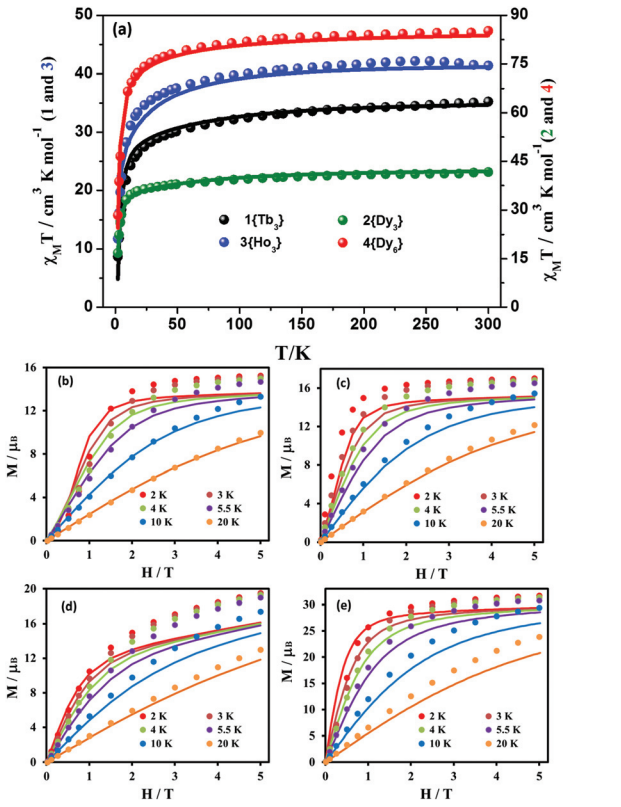

Fig. 4 (a) $\chi_M T$ *vs.* T plots for **1–4** in an applied dc magnetic field of 1 T. The measured molar magnetization data for (b) **1**$\{Tb_3\}$; (c) **2**$\{Dy_3\}$;[13] (d) **3**$\{Ho_3\}$ and (e) **4**$\{Dy_6\}$. The solid lines are POLY_ANISO fits of the data (see text in the theoretical section).

an S-shape profile at low magnetic fields (0–2.5 T) at 2 K (Fig. S5‡), indicating the possible presence of toroidal magnetic behaviour (see theoretical section).

The magnetic data for **4** are shown in Fig. 4a and e and are plotted as $\chi_M T$ *versus* T. The room temperature value of 85.23 cm^3 K mol^{-1} is in good agreement with the sum of the Curie constants for six non-interacting Dy^{III} ions of 85.02 cm^3 K mol^{-1}. As the temperature is decreased the $\chi_M T$ product decreases gradually down to 20 K, before a sharper drop below this temperature, reaching a value of 28.40 cm^3 K mol^{-1} at 2 K. Again, the decrease over the whole temperature range is due to the depopulation of the crystal field split Stark sublevels of the ground state, with possible weak intramolecular antiferromagnetic exchange and/or dipolar interactions contributing to the behaviour (see theoretical analysis). The isothermal *M versus H* plots are shown in Fig. 4 and Fig. S6.‡ Like **1**, however to a lesser extent, we observe an S-shape profile at low magnetic fields (0–1.5 T) at 2 K, indicating the possible presence of toroidal magnetic behaviour (see theoretical section). The $\chi_M T$ and M/H plots are generally similar to those displayed by our other Dy_6 rings.[4b,c]

To probe for any slow magnetic relaxation, ac susceptibility measurements were performed with an oscillating ac field of 3.5 Oe under a zero applied dc field. No out-of-phase ac susceptibility signals were observed for **1–3** in zero magnetic field, however out-of-phase peaks are observed for **4** between 2 and 4 K (Fig. S7,‡ left). Fitting the data to the Arrhenius law [$\tau = \tau_0 \exp(U_{eff}/k_B T)$] reveals that for T = 2.2–3.6 K, the plot is linear, yielding an anisotropy barrier U_{eff} = 14.7(1) K (~10 cm^{-1}), with $\tau_0 = 1.8 \times 10^{-6}$ s (Fig. S7,‡ right). At the lowest temperature, however, the plot deviates from linearity indicating QTM relaxation is active. To quench the QTM and slow the relaxation times we performed an isothermal (4 K) magnetic field sweep to find the optimum field with the longest relaxation time at that temperature. This was found to be 3000 Oe (Fig. S8‡). The frequency (0.1–1500 Hz) and temperature (2–12 K) dependent out-of-phase susceptibilities and Cole–Cole measurements for **4** at H_{dc} = 3000 Oe are shown in Fig. 5, top. We see that the ln (τ) *vs.* T^{-1} plot is linear between 9.5–12 K, below these temperatures the plot becomes non-linear, indicating a cross over from a thermally activated to a quantum assisted relaxation process.

Fitting the relaxation data[27] yielded the relaxation times with the various relaxation processes (Fig. 5, bottom) when using the following equation,

$$1/\tau = 1/\tau_{QTM} + AT + CT^n + {\tau_0}^{-1} \exp(U_{eff}/k_B T)$$

where $1/\tau_{QTM}$ corresponds to the relaxation process *via* QTM pathway, the AT term relates to the direct relaxation process, the CT^n term corresponds to the relaxation *via* a Raman process, and the last term accounts for the Orbach relaxation pathway.[22m,26d,28] The values obtained from the best fit are A = 6.9, n = 3.9, C = 0.096 s^{-1} $K^{-3.9}$, U_{eff} = 91.8 K and $\tau_0 = 1.02 \times 10^{-7}$ s (R = 0.9999) for **4**. Whereas the τ_{QTM} is considered to be 0 while fitting the data because the magnetic relaxation is dominated by direct and Raman processes upon application of a dc field of 3000 Oe for **4**. The n value is lower than expected which might be due to the presence of optical and acoustic Raman processes.[29]

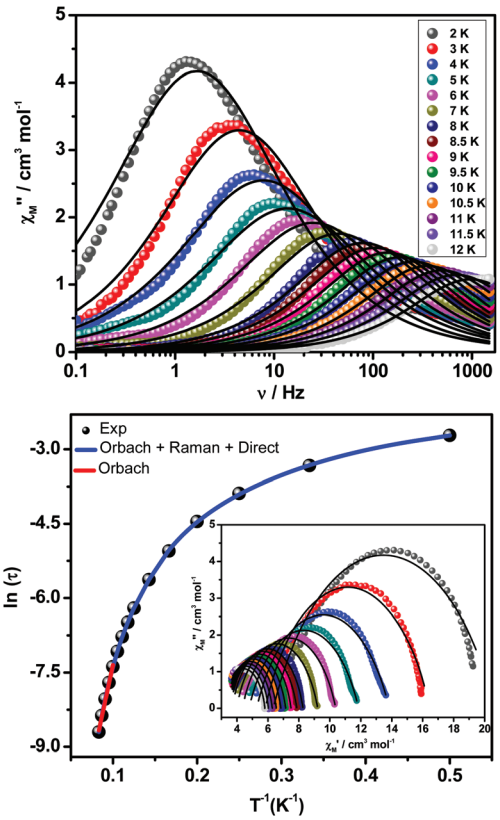

Fig. 5 (Top) χ''_M *vs.* frequency plots for **4** in an applied dc field H_{dc} = 3000 Oe, between 2–12 K. The solid black lines are fitted values obtained from the CC-fit program.[27] (Bottom) Relaxation time (τ), plotted as ln(τ) *versus* T^{-1} for **4**. The solid red line corresponds to fitting to an Orbach relaxation process and the solid blue line represents the best fitting to the multiple relaxation process. (Inset) Cole–Cole plot for **4**.

Theoretical analysis

The nature of the magnetic anisotropy of each Ln^{III} ion, the mechanism of single-ion/exchange-coupled magnetic relaxation and the observation/prediction of toroidal behaviour in both the triangular $\{Ln^{III}_3\}$ (Ln = Tb (**1**), Dy (**2**) and Ho (**3**)) and hexagonal wheel $\{Dy^{III}_6\}$ (**4**) systems were analysed using the MOLCAS 8.0 program[17] harnessing the CASSCF/RASSI-SO/SINGLE_ANISO/POLY_ANISO routine *ab initio* calculations (see computational details in the Experimental section and ESI‡). We first discuss the relaxation mechanism computed for the single Ln^{III} ions and then expand this to the exchanged coupled polynuclear complex.

Single ion calculations

The computed g-tensors and the energy values suggest that all Ln^{III} ions are symmetrically equivalent in **1–4** (see Table 1 and Tables S5–S19 in the ESI‡). The energy spectrum and g-tensors for the Ising doublets of the ground $^7F_6$ multiplet of three Tb^{III} sites in **1**$\{Tb_3\}$ is given in Table 1 and Tables S5–S7 in ESI,‡

Table 1 Low-lying energies (cm^{-1}) and *g*-tensors of Ln1 fragments of **1–4** that originate from the corresponding ground atomic multiplets

	1{Tb_3}	**2**{Dy_3}	**3** {Ho_3}	**4**{Dy_6}
	0.0	0.00	0.0	0.0
	0.18	112.1	2.8	108.1
	166.6	169.1	20.5	221.3
	179.3	250.8	26.6	281.5
	199.1	315.1	70.3	338.2
	225.1	356.6	76.2	444.9
	281.0	446.3	117.3	562.9
	325.6	554.7	128.4	680.9
	342.8		150.9	
	437.5		183.3	
	442.4		202.5	
	513.0		216.8	
	515.1		222.8	
g_{xx}	0.0000	0.0600	0.0000	0.0134
g_{yy}	0.0000	0.1100	0.0000	0.0213
g_{zz}	17.8100	19.6600	17.1300	19.8178

with subsequent excited state multiplets lying 2120 cm^{-1} above the ground multiplet. The ground and excited pseudo-doublets exhibit pure Ising type anisotropy for all the symmetrically equivalent magnetic sites. The g_z parameter of the ground pseudo-doublet state (see Fig. 6a, yellow dashed lines for the orientation of the ground state anisotropy axis) is close to that expected for a pure $m_J = \pm 6$ states (see Tables S5–S7‡). In all the equivalent sites, a substantial Δ_{tun} (>10^{-5} cm^{-1}) within the ground pseudo-doublets was detected (~0.2 cm^{-1}). To understand the origin of such splitting, crystal field analysis were performed which indicate predominantly large axial terms (see Table S8‡), however, the competitive nature of the non-axial terms suppresses the dominant axiality. Therefore, both the prevalent non-axial crystal field parameters in conjunction with a large tunnel splitting within ground pseudo-doublets preclude any SMM characteristics, due to quantum tunnelling relaxation mechanism originating in the ground state. This analysis is complemented experimentally by the lack of out-of-phase susceptibility signals from the ac measurements.

The energy levels and *g*-tensors for the Kramers doublets of the ground $^6H_{15/2}$ multiplet of the three Dy^{III} sites in the **2**{Dy_3} complex, are shown in Table 1 and Tables S9–S11,‡ with subsequent excited multiplet states lying ~3090 cm^{-1} above the ground muliplet. The ground state (GS) Kramers doublet shows an axial type anisotropy for all the three metal centres (see Table 1 and Tables S9–S11‡) *i.e.* g_{zz} (see Fig. 6b, yellow dashed lines for the orientation of the main anisotropy axis for the ground KD in all three Dy^{III} sites) is close to that expected for a pure $m_J = \pm 15/2$ state (g_x = 0.06, g_y = 0.11, g_z = 19.66). For each Dy^{III} ion, the angle between g_z directions of the ground and first excited KD is estimated to be ~104°. It indicates that the magnetic relaxation to be operative *via* the first excited KD in all three equivalent Dy^{III} centres. Therefore, based on single-ion analysis, the computed energy barrier for magnetization reversal (U_{cal}) can be enumerated as 112 cm^{-1} for all the three symmetrically equivalent Dy^{III} centres. This, therefore, suggests SMM behaviour is possible for complex **2**.

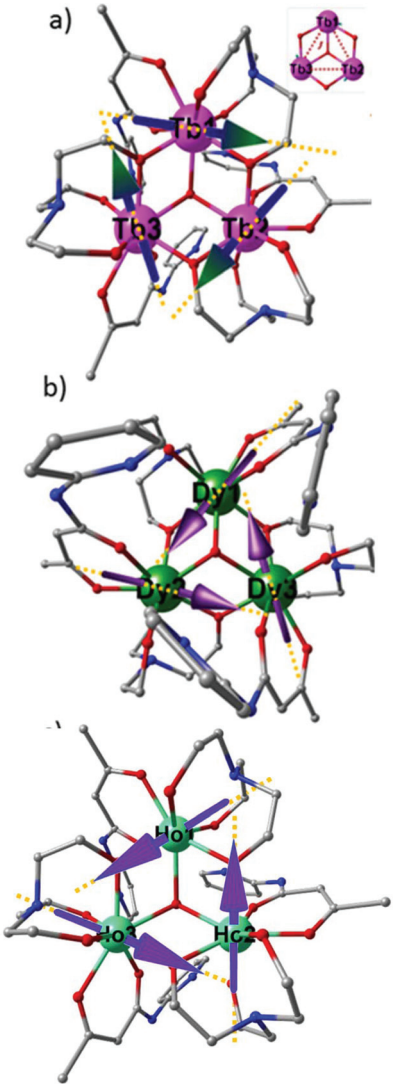

Fig. 6 The directions of the local anisotropy axes in the ground doublets on the Ln^{III} sites (yellow dashed lines) and of the local magnetic moments (colour arrows) in the ground exchange doublet of (a) **1**{Tb_3}; (b) **2**{Dy_3}; (c) **3**{Ho_3}.

However, the presence of large non-axial crystal field parameters (see Table S12‡) indicate prominent QTM effects in the ground state which can lead to a lack of SMM behaviour in **2**. This agrees well with the experimental observation of an absence of a frequency dependent out-of-phase magnetic susceptibility signal in zero dc field.

The energy levels and *g*-tensors for the Ising doublets of the ground $^5I_8$ multiplet of the three Ho^{III} sites in **3**{Ho_3} are shown in Table 1 and Tables S13–S15,‡ with subsequent excited multiplet states lying ~5275 cm^{-1} above the ground multiplet. The ground and excited state pseudo-doublets exhibit pure Ising type anisotropy for all three equivalent Ho^{III} sites owing to the overall non-Kramers nature of the Ho^{III} centres. The ground state g_z value (see Fig. 6c, yellow dashed lines for the orientation of main anisotropy axis for the ground pseudo-doublet for all three Ho^{III} sites) is close to

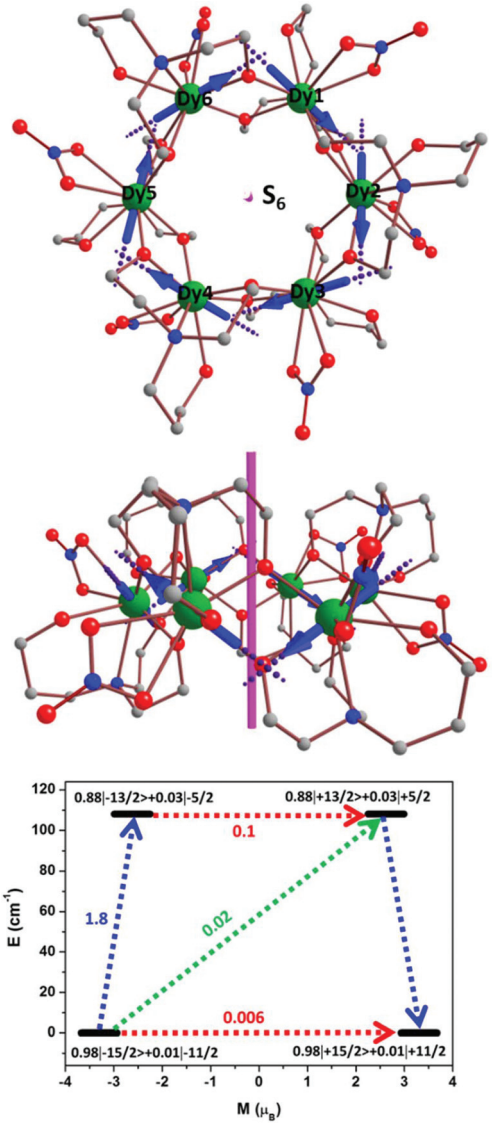

Fig. 7 (Top) The directions of the local anisotropy axes in the ground doublets on the Ln^{III} sites (violet dashed lines) and of the local magnetic moments (blue arrows) in the ground exchange doublet of **4**{Dy_6}. The S_6 axis is shown as a pink bold line. (Middle) side view of **4**{Dy_6}. (Bottom) The computed blocking barrier for the Dy1 site in **4**{Dy_6}. The thick black line indicates the Kramer's doublets as a function of computed magnetic moment. The green/blue arrows show the possible pathway through Orbach/Raman relaxation. The dotted red lines represent the presence of QTM/TA-QTM between the connecting pairs. The numbers provided at each arrow are the mean absolute value for the corresponding matrix element of transition magnetic moment.

that expected for a pure m_J = ±8 state (see Table 1 and Tables S13–15‡). Based on the single-ion analysis, a pronounced Δ_{tun} was computed within the ground pseudo-doublets (~3 cm^{-1} *i.e.* >cut-off of 10^{-5} cm^{-1}) for all Ho^{III} sites. This restricts the observation of SMM behaviour in **3**. Substantial non-axial crystal field parameters (see Table S16‡) further corroborated the lack of SMM behaviour in **3** from experiment.

The local *g*-tensors of each Dy^{III} ion in the ground Kramers doublet of **4** (Dy^{III}_6) are strongly axial in nature (Table 1 and Table S17‡) indicating the possibility of slow magnetic relaxation originating from the single ion. The orientations of the main anisotropy axes in the ground KDs of **4** is shown in Fig. 7, top and middle. The computed energy gap between the ground KDs and the excited states for **4** are shown in Table 1 and Table S18.‡ In complex **4**, the energy gap between the ground and the first excited KD is calculated to be ~108 cm^{-1} for all the Dy^{III} ions.

A qualitative mechanism for the single ion magnetic relaxation for Dy1 is shown in Fig. 7, bottom and a similar kind of mechanism is observed for other Dy^{III} ions. The ground-state tunnelling probability (QTM) is small, becoming larger in the first excited states for all Dy^{III} ions, therefore single-ion magnetic relaxation can occur *via* first excited states involving thermally assisted QTM. The computed barrier can be compared with the experimental out-of-phase ac measurements at a static dc field of 3000 Oe (U_{eff} = 91.8 K), which is slightly less than calculated indicating under barrier relaxation pathways are operational even in the presence of a static dc field.

Exchange-coupled magnetic relaxation and toroidal behaviour

The magnetic exchange and dipolar interactions between nearest-neighbour Ln^{III} sites of **1–4** were simulated using the POLY_ANISO program[24] and the values are listed in Table 2. By considering the exchange constants (J_{exch} + J_{dip}) values, good fits to both the susceptibility and the magnetization data were attained for both triangular and wheel systems (Fig. 4). The *M vs. H* fit however reveal some deviation at high-field and this could be due to the limited number of roots that are considered for our simulations due to very large structures.

Pure Ising type pseudo-doublets associated with all the Tb^{III} centres in **1** is indicative of the possibility of an Ising type magnetic interaction between the Tb^{III} centres. We have simulated the magnetic exchange coupling between the Tb^{III} ions, including the magnetic dipole–dipole, as well as the exchange interaction contributions within the Ising exchange Hamiltonian, harnessing the POLY_ANISO suite. Experimental magnetic data ($\chi_M T$ (T) and $M(H)$) were reproduced nicely through our simulations with the J_{exch} = −0.06 cm^{-1} and without the *zJ* parameters (Fig. 4a, b and Table 2).

Taking into account the Ising type exchange interaction, the following Hamiltonian becomes applicable:

$$\widetilde{H_{ex}} = -\sum_{i=1}^{3} \tilde{J}_i \tilde{S}_{iz} \tilde{S}_{i+1z};$$

where $\tilde{S}_{iz}$ represents pseudo-spin projection on the anisotropy axis of the i^{th} centre and also illustrates two states with

Table 2 POLY_ANISO[24] fitted exchange and dipolar couplings (cm^{-1}) between Ln^{III}–Ln^{III} ions of **1–4**. Here *zJ* (cm^{-1}) is the intermolecular exchange interaction

Complex	J_{exch}	J_{dip}	J_{tot}	*zJ*
1	−0.06	−0.19	−0.25	0
2	−0.35	+0.07	−0.28	0
3	−0.67	+0.11	−0.56	0
4	−0.10	+1.10	+1.00	−0.01

reversed maximal magnetization on this magnetic site. Concepts based on the Lines model and the above Hamiltonian have aided derivation of the equation: $\tilde{J}_i = 25\cos\phi_{i,j+1}J_i$. Here, $\phi_{i,j+1}$ corresponds to the angle between the anisotropy axes on the centres i and $i+1$. As $\phi_{i,j+1} \sim 2\pi/3$, $\tilde{J}_i = -12.5J_i$. This approximation resulted in positive $\tilde{J}$ between Tb^{III} centres for antiferromagnetic J, as observed in **1** (see Table 2). This produces a ferromagnetic alignment of the pseudospins (bluish-green arrows in Fig. 6a) which is collinear with the direction of the main anisotropy axis (dashed yellow lines in Fig. 6a). Moreover, the local magnetization vectors are found to almost lie in the $\{Tb_3\}$ plane with an out-of-plane angle in the range of 2° (see Table S19‡). Besides, they are almost tangential to the vertices of the $\{Tb^{III}_3\}$ triangle, which exemplifies **1** as a complex exhibiting an almost perfect toroidal magnetic moment (see Fig. 6a).

Next, we attempt to analyse the overall non-Kramers type exchange coupled system in **1** *i.e.* overall $|M_J\rangle = 6 \times 3 = 18$ states. Due to the non-Kramers nature of the Tb^{III} ion, all the exchange pseudo-doublets possess almost negligible matrix elements of the transversal magnetic moment ($\sim 10^{-5}$–$10^{-9}\mu_B$) pertinent to QTM/TA-QTM processes but differ significantly in terms of tunnel splitting (see Table 3). A prominent Δ_{tun} of $\sim 10^{-4}$ cm^{-1} (higher than the cut-off of $\sim 10^{-5}$ cm^{-1}) was detected within the ground pseudo exchange doublet in **1**. This results in fast relaxation of magnetization through ground exchange state itself (see Fig. 8a) negating any SMM behaviour. Despite three symmetrically equivalent Tb^{III} sites, the magnetic moments of the Tb^{III} ions do not compensate completely. Rather, they sum up to a total momentum of $\mu_z = 1/2\ g_z\mu_B = 0.87\mu_B$ in the ground exchange pseudo-doublet, which is much smaller than the magnetic moment on each Tb^{III} site in the ground state *i.e.* $9\mu_B$. From Fig. 4a, the $\chi_M T$ value diminishes at low temperature (both the POLY_ANISO fit and the experimental data) denoting a non-magnetic ground state. However, the non-collinear exchange between localized magnetic moments does not compensate each other completely resulting in a small residual ground pseudo exchange doublet magnetic moment. This accords well with the non-zero magnitude of magnetization even at low temperature, as evident from Fig. 4e, and is reminiscent of earlier reports on Dy_3 triangles.[2a,22l,30] Therefore, we can conclude that complex **1** is not a SMM but shows mixed moment type SMT behaviour.

Similar to the earlier explanation, a nice agreement between experimental and POLY_ANISO simulated magnetic

Table 3 Energies (cm^{-1}), corresponding tunnel splitting (Δ_{tun}) and g_z values of the low-lying exchange doublet state in complex **1**

Multiplets	Energy (cm^{-1})	Main values of g tensor		Δ_{tun} (cm^{-1})
1	0.0000	g_{xx}	1×10^{-9}	0.0005
	0.0000	g_{yy}	2×10^{-9}	
		g_{zz}	1.74	
2	3.841	g_{xx}	3×10^{-7}	0.0788
	3.920	g_{yy}	2×10^{-5}	
		g_{zz}	25.26	
3	3.925	g_{xx}	2×10^{-7}	0.1696
	4.094	g_{yy}	9×10^{-6}	
		g_{zz}	17.95	
4	4.099	g_{xx}	4×10^{-7}	0.0903
	4.189	g_{yy}	2×10^{-5}	
		g_{zz}	25.25	
5	168.311	g_{xx}	9×10^{-8}	0.0135
	168.325	g_{yy}	2×10^{-6}	
		g_{zz}	8.266	

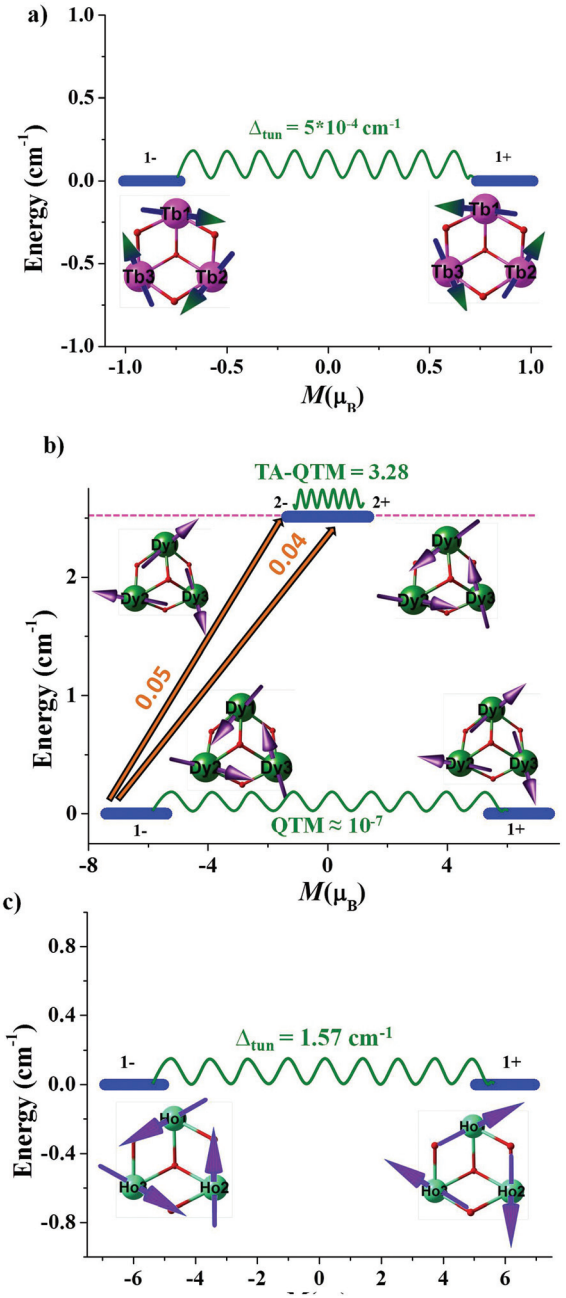

Fig. 8 Low-lying exchange energies in complex (a) **1**$\{Tb_3\}$; (b) **2**$\{Dy_3\}$; (c) **3**$\{Ho_3\}$. Every exchange state (represented by thick blue lines) has been arranged based on the corresponding magnetic moment. The curved green arrows indicate a tunnelling transition (Δ_{tun}; tunnel splitting or tunnel gaps) within each doublet. At a few energy levels the corresponding non-collinear Ising quantum states, with thick arrows at the Ln^{III} sites, indicate magnetic moment directions in toroidal form.

data (see Fig. 4a and c) was established with $J_{exch} = -0.35$ cm^{-1} in complex **2** (see Table 2). This approximation leads to positive $\tilde{J}$ between Dy^{III} centres for antiferromagnetic J (see Table 2). This leads to the ferromagnetic alignment of the pseudospins (purple arrows in Fig. 6b) which is collinear with the direction of the main anisotropy axis (yellow dashed lines in Fig. 6b). Moreover, the local magnetization vectors are found to lie close to the $\{Dy_3^{III}\}$ plane, with an out-of-plane angle in the range of 13° (see Table S19‡). Besides, they are almost tangential to the vertices of the $\{Dy_3^{III}\}$ triangle which reveals complex **2** exhibits a toroidal magnetic moment (see Fig. 6b). Next, we analyse the Kramers type exchange system for **2** *i.e.* overall $|M_J\rangle$ = 15/2 × 3 = 45/2 states. Due to the Kramers nature of the Dy^{III} ion, all the exchange Kramers doublets possess almost negligible matrix tunnel splitting between them (~10^{-9}–10^{-11} cm^{-1}; see Table 4). Since the exchange-coupled $|M_J\rangle$ states are Kramers in nature, the matrix elements of the transversal magnetic moment (QTM/TA-QTM values) tend to dominate in predicting magnetic relaxation. The matrix element pertaining to the ground state QTM is negligible (less than the cut-off value of $10^{-3}\mu_B$; see Fig. 8b and Table 4). However, a substantial amount of matrix element corresponding to operative TA-QTM within the first excited exchange doublet (3.28μ_B; see Fig. 8b and Table 4) promotes relaxation *via* the first excited exchange doublet. This implies the computed energy barrier as 2.5 cm^{-1} for complex **2** supporting the observed absence of frequency dependent out-of-phase magnetic susceptibility (zero-field or in presence of field). Hence, the weak antiferromagnetic exchange interaction between Dy^{III} sites dominate enough to quench the QTM at the ground state at the single-ion level leading to possible relaxation in the polynuclear framework. However, due to the small barrier in the exchange coupled framework slow relaxation is not expected to be observed in line with the experimental magnetic data. Despite the three equivalent Dy^{III} sites, the magnetic moments of the Dy^{III} ions do not compensate completely. Rather, they sum up to a total momentum of μ_z = 1/2 $g_z\mu_B$ = 6.40μ_B in the ground exchange pseudo-doublet, which is much smaller than the magnetic moment on each Dy^{III} site in the ground state, *i.e.* 10μ_B. From Fig. 4a, the $\chi_M T$ value diminishes at low temperature, but to a lesser extent than **1**. Non-collinear exchange between localized magnetic moments does not compensate each other resulting in a small residual ground pseudo exchange doublet magnetic moment (larger than **1**). This accords well with the non-zero magnetization value even at low temperature as evident from Fig. 4c and is reminiscent of earlier reports on $\{Dy_3\}$ triangles.[2a,22l,30] Therefore, we can conclude that, complex **2** is not an SMM, but shows mixed moment type SMT behaviour.

The POLY_ANISO simulation revealed $J_{exch} = -0.67$ cm^{-1} for **3** (see Fig. 4a, d and Table 2). This is similar to the outcomes calculated from the **1**$\{Tb_3\}$ and **2**$\{Dy_3\}$ triangles and with a ferromagnetic alignment of the local magnetization vectors on the three Ho^{III} centres. The spins form an 18–20° angle with the $\{Ho_3\}$ plane and almost tangential orientation of these local magnetization vectors induce SMT behaviour in **3**. Next, we have explored the non-Kramers type exchange coupled system in **3** *i.e.* overall $|M_J\rangle$ = 8 × 3 = 24 states. All the exchange pseudo-doublets possess negligible matrix elements of the transversal magnetic moment (~10^{-6}–$10^{-9}\mu_B$) corresponding to QTM/TA-QTM but differ significantly in terms of tunnel splitting (see Table 5). A prominent Δ_{tun} = 1.57 cm^{-1} (higher than the cut-off of ~10^{-5} cm^{-1}) was detected within the ground pseudo exchange doublet. This results in fast relaxation of magnetization through the ground exchange state (see Fig. 8b), precluding any SMM behaviour. Despite three symmetrically equivalent Ho^{III} sites, the magnetic moments of the Ho^{III} ions in **3** do not compensate completely. Rather, they sum up to a total momentum of μ_z = 1/2$g_z\mu_B$ = 5.98μ_B in the ground exchange pseudo-doublet which is much smaller than the magnetic moment on each Ho^{III} site in the ground states *i.e.* 9μ_B. From Fig. 4a, the $\chi_M T$ value diminishes at low temperature but less so than in **1** and similar to the behaviour in **2**. Non-collinear exchange between localized magnetic moments does not compensate each other resulting in small residual ground pseudo exchange doublet magnetic moment (larger

Table 4 Energies (cm^{-1}), corresponding tunnel splitting (Δ_{tun}) and g_z values of the low-lying exchange doublet state in complex **2**

Multiplets	Energy (cm^{-1})	Main values of g tensor		Δ_{tun} (cm^{-1})
1	0.0000	g_{xx}	1×10^{-7}	1×10^{-10}
	0.0000	g_{yy}	4×10^{-7}	
		g_{zz}	12.80	
2	2.506	g_{xx}	24.56	1×10^{-10}
	2.506	g_{yy}	13.41	
		g_{zz}	0.06	
3	2.535	g_{xx}	0.02	3×10^{-11}
	2.535	g_{yy}	3.91	
		g_{zz}	11.78	
4	2.563	g_{xx}	25.42	1×10^{-10}
	2.563	g_{yy}	12.87	
		g_{zz}	0.06	
5	109.686	g_{xx}	6×10^{-5}	1×10^{-9}
	109.686	g_{yy}	1×10^{-4}	
		g_{zz}	22.62	

Table 5 Energies (cm^{-1}), corresponding tunnel splitting (Δ_{tun}) and g_z values of the low-lying exchange doublet state in complex **3**

Multiplets	Energy (cm^{-1})	Main values of g tensor		Δ_{tun} (cm^{-1})
1	0.000	g_{xx}	1×10^{-7}	1.573
	1.573	g_{yy}	4×10^{-7}	
		g_{zz}	12.80	
2	3.706	g_{xx}	6×10^{-7}	0.350
	4.056	g_{yy}	2×10^{-6}	
		g_{zz}	0.29	
3	4.937	g_{xx}	2×10^{-7}	1.656
	6.593	g_{yy}	1×10^{-6}	
		g_{zz}	0.13	
4	7.000	g_{xx}	3×10^{-8}	2.195
	9.195	g_{yy}	9×10^{-7}	
		g_{zz}	21.48	
5	18.692	g_{xx}	5×10^{-8}	0.309
	19.001	g_{yy}	2×10^{-7}	
		g_{zz}	0.22	

Table 6 Summary of results of **1–3** from *ab initio* calculations

		SMT		
Complexes	SMM	Type	T_z	M/μ_B
1	No	Yes, mixed moment	≠0	0.87
2	No	Yes, mixed moment	≠0	6.40
3	No	Yes, mixed moment	≠0	5.98

than **1**). This accords well with the non-zero magnitude of magnetization even at low temperature as evident from Fig. 4d and is reminiscent of earlier reports on $\{Dy_3\}$ triangles.[2a,22l,30] Therefore, we can conclude that complex **3** is not an SMM but shows mixed moment type SMT behaviour.

Hence, our theoretical analysis on complexes **1–3** leads to the following summary (Table 6):

Analysis of the exchange coupling for **4** reveals that the tilt angle (θ) between the orientation of the magnetic moments and the vector connecting two Dy^{III} centres is found to be ~38° which is lower than 54.75° which can decide the nature of dipolar interaction.[31] This lesser angle causes a ferromagnetic dipolar contribution to the net magnetic exchange.

In **4**, the tunnelling gap of the ground exchange coupled states is small becoming larger at the first and second excited states (Fig. 9). Furthermore, Table S20‡ shows that those coupled excited states are very close in energy resulting in fast relaxation of magnetization *via* second excited states at 4.2 cm^{-1}. This lies in line with the small observed anisotropy barrier (~10 cm^{-1}) as determined experimental out-of-phase ac magnetic susceptibilities in a zero static dc field.

The direction of the local anisotropy axes on all Dy^{III} sites is shown in Fig. 7 (top and middle), by dashed lines. The angle

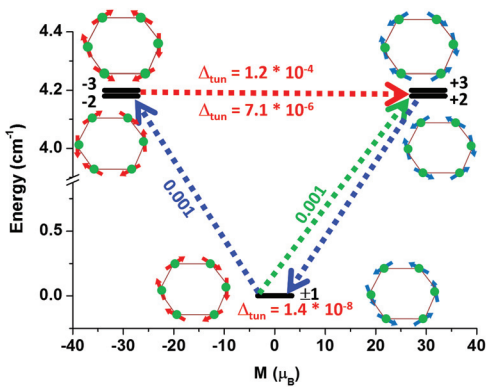

Fig. 9 Low-lying exchange energy levels in **4** $\{Dy_6\}$. The exchange states are placed on the diagram according to their magnetic moments (bold black lines). Red arrows show the tunnelling transitions within each doublet state, while green/blue arrows show the possible pathway through Orbach/Raman relaxation. The numbers at the paths are averaged transition moments in μ_B, connecting the corresponding states. At a few energy levels, it provides a graphical representation of one of the corresponding non-collinear Ising quantum states, where the red/blue thick arrows at the Ln^{III} sites indicate magnetic moment direction in toroidal form.

of these axes with the main symmetry axis of the **4**$\{Dy_6\}$ complex (S_6) is 84°. The direction of the main anisotropy axes on each Dy^{III} ion are following each other, thus forming a circular pattern similar to earlier reported $\{Dy_6\}$[4b,c] complexes, resulting in a toroidal magnetic moment. The presence of ferromagnetic dipolar coupling and the S_6 symmetry of the complexes results in a negligible (or zero) magnetic moment ($0.0003\mu_B$) in the ground coupled states, again similar to that reported for other $\{Dy_6\}$ examples.[4b,c] Thus, **4** is categorised as an SMT displaying a net toroidal moment.[32] Here, the ferromagnetic dipolar coupling is smaller (+1.1 cm^{-1}) compared to the reported antiferromagnetic dipolar coupling (−4.2 cm^{-1} and −9.2 cm^{-1}) for $\{Dy_6\}$.[4b,c] The extra $-CH_2-$ arm in the $teaH_3$ ligand ($pdeaH_3$) utilised in the synthesis of **4** results in a smaller tilt angle (θ = ~38° < 54.75°), which leads to the ferromagnetic dipolar coupling. Whereas this angle was found to be 73° and 87.4° for the parent $\{Dy_6\}$ complexes.[4b,c] The local anisotropy axes are found to be almost in the plane of the molecule, at 84° from the S_6 symmetry, however the smaller dipolar coupling does not improve the stabilization energy of the ground toroidal magnetic state that lies 4.2 cm^{-1} below the excited states (4.8 cm^{-1} and 4.4 cm^{-1} for previously reported $\{Dy_6\}$ complexes).[4b,c]

Toroidal magnetic behaviour of $\{Ln_3^{III}\}$ and $\{Ln_6^{III}\}$

The studied $\{Ln_3^{III}\}$ triangular and a $\{Dy_6^{III}\}$ wheel complexes satisfy the two necessary criteria required for a complex to display SMT behaviour: (a) the planar arrangement of local anisotropy axes and (b) the cyclic symmetry of the polynuclear Ln^{III} complex. Moreover, the exchange and dipolar interaction between lanthanide ions decide the stabilization energy of their toroidal magnetic states.

The toroidal magnetic moment in the ground state of **2** $\{Dy_3^{III}\}$ is $6.4\mu_B$ which is three-times smaller compared to that calculated for the first archetypal $\{Dy_3^{III}\}$ SMT, which has a value of $19.7\mu_B$. Our calculations also predict toroidal behaviour for $\{Tb_3^{III}\}$ and $\{Ho_3^{III}\}$ triangles. The presence of conventional magnetic moments of $0.9\mu_B$, $6.4\mu_B$ and $6.0\mu_B$ with C_3 symmetry for **1**, **2** and **3**, respectively makes them mixed-moment SMTs.[32] Whereas, previously reported $\{Tb_6\}$, $\{Dy_6\}$ and $\{Ho_6\}$ wheels possess negligible or no magnetic moments of $0.4\mu_B$, $0.003–0.005\mu_B$ and $0.5\mu_B$, respectively with higher S_6 symmetry makes them net toroidal moment SMTs.[4b,c] Toroidal behaviour is rare in non-Kramer ions and thus **1** and **3** are the first non-Kramer type mixed-moment type SMTs.

We show with **4** that by chemically modifying the amine polyalcohol ligand ($pdeaH_3$ *vs.* $teaH_3$) we can modify the magnetic behavior in two ways. Firstly, we observe that minor changes of the ligand field shift the toroidal magnetic stabilization energy. However, we observe a reduction in the stabilization energy for **4** (toroidal ground to non-toroidal excited state) compared to our earlier reported $\{Dy_6\}$ wheels.[4b,c] If we can achieve a larger tilt angle (θ) than that observed for the parent $\{Dy_6\}$ complex, then a greater energy separation is expected.[4b,c] Unfortunately, for **4**, a smaller tilt angle resulted in weak ferromagnetic dipolar coupling, reducing the toroidal

ground state stabilisation energy. We do note, however, that **4** shows a larger stabilization energy (4.2 cm^{-1}) compared to the {Dy_6} wheel reported by Powell *et al.* utilizing the ligand 2,2′-(3-aminopropylazanediyl)diethanol (apadH_4), reported as 2.1 cm^{-1} (3 K).[4a] Since the stabilization energy was not calculated using *ab initio* calculations, we compared the magnetization blockade value of their {Dy_6} complex estimated using ac plots and it is noteworthy that the stabilization energy of toroidal magnetic states could not be more than this. Secondly, an imaginary component for **4** is observed in the ac susceptibility curves, as seen for previously reported {Dy_6} wheels.[4b,c] However, whereas the previous {Dy_6} complexes do not show any peak maxima in the χ'' *vs.* *T* curves, compound **4** has a significantly higher blocking temperature, showing a well-defined maximum in χ'' under zero and a 3000 Oe applied dc field. We, therefore, show that minor modifications of the ligand field can improve SMM properties. We see that the improved SMM behaviour, shown from the experiment for **4**, is in line with our *ab initio* analysis as **4** displays the smallest energy gap between the toroidal and ferromagnetic states (4.2 cm^{-1} *vs.* 4.8 and 4.4 cm^{-1}). As the non-magnetic zero-field ground state cannot support the slow relaxation, the SMM properties are superior when the ferromagnetic arrangement is achieved and these are easier to achieve when the aforementioned gap is smaller as seen in the case of **4**.

Conclusions

We report the synthesis, magnetic properties and theoretical predictions of three triangular complexes, $[Ln^{III}_3(OH)(teaH_2)_3(paa)_3]Cl_2$ (Ln = Tb (**1**), Dy (**2**)[13] and Ho (**3**)), and a new wheel-type compound $[Dy^{III}_6(pdeaH)_6(NO_3)_6]$ (**4**). The *M* *vs.* *H* plots for **1** and **4** revealed an S-shaped curve, in low fields at 2 K, indicative of the presence of a toroidal moment, whereas, such an S-shape was not observed for **2** and **3**. However, *ab initio* calculations suggest a toroidal behaviour for all four complexes. The triangular complexes **1–3** display a mixed moment type SMT behaviour and the hexanuclear wheel **4** displays a net toroidal magnetic moment. The stabilization energy of the toroidal magnetic state in {Dy_6} (**4**) is found to be 4.2 cm^{-1} which is smaller compared to the earlier reported {Dy_6} complexes (4.4 cm^{-1} and 4.8 cm^{-1})[4b,c] due to weaker ferromagnetic dipolar coupling. The small energy difference (2.5 cm^{-1} for **2** and 1.57 cm^{-1} for **3**) between the ground and the first excited exchange doublet states, and the presence of large magnetic moment of the first excited exchange doublet gives an explanation for why the low-field *M* *vs.* *H* data do not show an S-shape for **2** and **3**. Our combined theoretical and experimental studies suggest that *ab initio* calculations are key in determining the toroidal behaviour in molecular complexes. While other unambiguous experimental determinations of such toroidal states, using, for example NMR spectroscopy have been proposed, such measurements are very rare on such systems and are urgently needed to offer insight into the toroidal magnetic behaviour of various lanthanide clusters.

Conflicts of interest

There are no conflicts to declare.

Acknowledgements

GR would like to thank SERB (CRG/2018/000430) for funding and IIT Bombay for high-performance computing facilities. KSM thanks the Australian Research Council for funding. KRV thanks the IIT Bombay for a Research Associate (RA) position. TG is indebted to the UGC (India) for providing financial assistance to conduct research activities.

References

1 J. Tang, I. Hewitt, N. T. Madhu, G. Chastanet, W. Wernsdorfer, C. E. Anson, C. Benelli, R. Sessoli and A. K. Powell, *Angew. Chem., Int. Ed.*, 2006, **45**, 1729–1733.
2 (*a*) L. F. Chibotaru, L. Ungur and A. Soncini, *Angew. Chem., Int. Ed.*, 2008, **47**, 4126–4129; (*b*) S.-Y. Lin, W. Wernsdorfer, L. Ungur, A. K. Powell, Y.-N. Guo, J. Tang, L. Zhao, L. F. Chibotaru and H.-J. Zhang, *Angew. Chem., Int. Ed.*, 2012, **51**, 12767–12771; (*c*) A. Soncini and L. F. Chibotaru, *Phys. Rev. B: Condens. Matter Mater. Phys.*, 2008, **77**, 220406; (*d*) P.-H. Lin, T. J. Burchell, L. Ungur, L. F. Chibotaru, W. Wernsdorfer and M. Murugesu, *Angew. Chem., Int. Ed.*, 2009, **48**, 9489–9492; (*e*) D. Gatteschi, R. Sessoli and L. Sorace, in *Handbook on the Physics and Chemistry of Rare Earths*, ed. G. B. Jean-Claude and K. P. Vitalij, Elsevier, 2016, vol. 50, pp. 91–139; (*f*) J. Luzon, K. Bernot, I. J. Hewitt, C. E. Anson, A. K. Powell and R. Sessoli, *Phys. Rev. Lett.*, 2008, **100**, 247205; (*g*) M. Gysler, F. El Hallak, L. Ungur, R. Marx, M. Hakl, P. Neugebauer, Y. Rechkemmer, Y. Lan, I. Sheikin, M. Orlita, C. E. Anson, A. K. Powell, R. Sessoli, L. F. Chibotaru and J. van Slageren, *Chem. Sci.*, 2016, **7**, 4347–4354.
3 (*a*) A. I. Popov, D. I. Plokhov and A. K. Zvezdin, *Phys. Rev. B: Condens. Matter Mater. Phys.*, 2016, **94**, 184408; (*b*) C. Das, S. Vaidya, T. Gupta, J. M. Frost, M. Righi, E. K. Brechin, M. Affronte, G. Rajaraman and M. Shanmugam, *Chem. – Eur. J.*, 2015, **21**, 15639–15650.
4 (*a*) A. Baniodeh, N. Magnani, S. Brase, C. E. Anson and A. K. Powell, *Dalton Trans.*, 2015, **44**, 6343–6347; (*b*) S. K. Langley, K. R. Vignesh, B. Moubaraki, G. Rajaraman and K. S. Murray, *Chem. – Eur. J.*, 2019, **25**, 4156–4165; (*c*) L. Ungur, S. K. Langley, T. N. Hooper, B. Moubaraki, E. K. Brechin, K. S. Murray and L. F. Chibotaru, *J. Am. Chem. Soc.*, 2012, **134**, 18554–18557.
5 G. Fernandez Garcia, D. Guettas, V. Montigaud, P. Larini, R. Sessoli, F. Totti, O. Cador, G. Pilet and B. Le Guennic, *Angew. Chem., Int. Ed.*, 2018, **57**, 17089–17093.
6 G. Novitchi, G. Pilet, L. Ungur, V. V. Moshchalkov, W. Wernsdorfer, L. F. Chibotaru, D. Luneau and A. K. Powell, *Chem. Sci.*, 2012, **3**, 1169–1176.

7 J. Wu, X.-L. Li, M. Guo, L. Zhao, Y.-Q. Zhang and J. Tang, *Chem. Commun.*, 2018, **54**, 1065–1068.
8 K. R. Vignesh, A. Soncini, S. K. Langley, W. Wernsdorfer, K. S. Murray and G. Rajaraman, *Nat. Commun.*, 2017, **8**, 1023.
9 (*a*) X.-L. Li, J. Wu, J. Tang, B. Le Guennic, W. Shi and P. Cheng, *Chem. Commun.*, 2016, **52**, 9570–9573; (*b*) J. Lu, V. Montigaud, O. Cador, J. Wu, L. Zhao, X.-L. Li, M. Guo, B. Le Guennic and J. Tang, *Inorg. Chem.*, 2019, DOI: 10.1021/acs.inorgchem.9b01068; (*c*) S. Xue, X.-H. Chen, L. Zhao, Y.-N. Guo and J. Tang, *Inorg. Chem.*, 2012, **51**, 13264–13270.
10 K. R. Vignesh, S. K. Langley, A. Swain, B. Moubaraki, M. Damjanović, W. Wernsdorfer, G. Rajaraman and K. S. Murray, *Angew. Chem., Int. Ed.*, 2018, **57**, 779–784.
11 (*a*) E. Coronado and A. J. Epsetin, *J. Mater. Chem.*, 2009, **19**, 1670–1671; (*b*) M. N. Leuenberger and D. Loss, *Nature*, 2001, **410**, 789–793.
12 L. Bogani and W. Wernsdorfer, *Nat. Mater.*, 2008, **7**, 179–186.
13 S. K. Langley, B. Moubaraki and K. S. Murray, *Polyhedron*, 2013, **64**, 255–261.
14 G. Sheldrick, *Acta Crystallogr., Sect. A: Found. Crystallogr.*, 2008, **64**, 112–122.
15 G. M. Sheldrick, SHELXL-2018/3, *Acta Crystallogr., Sect. C: Struct. Chem.*, 2015, **71**, 3–8.
16 L. J. Barbour, *J. Supramol. Chem.*, 2001, **1**, 189–191.
17 F. Aquilante, J. Autschbach, R. K. Carlson, L. F. Chibotaru, M. G. Delcey, L. D. Vico, I. F. Galván, N. Ferré, L. M. Frutos, L. Gagliardi, M. Garavelli, A. Giussani, C. E. Hoyer, G. L. Manni, H. Lischka, D. Ma, P. Å. Malmqvist, T. Müller, A. Nenov, M. Olivucci, T. B. Pedersen, D. Peng, F. Plasser, B. Pritchard, M. Reiher, I. Rivalta, I. Schapiro, J. Segarra-Martí, M. Stenrup, D. G. Truhlar, L. Ungur, A. Valentini, S. Vancoillie, V. Veryazov, V. P. Vysotskiy, O. Weingart, F. Zapata and R. Lindh, *J. Comput. Chem.*, 2016, **37**, 506–541.
18 B. O. Roos, R. Lindh, P.-A. Malmqvist, V. Veryazov, P.-O. Widmark and A. C. Borin, *J. Phys. Chem. A*, 2008, **112**, 11431–11435.
19 B. A. Hess, C. M. Marian, U. Wahlgren and O. Gropen, *Chem. Phys. Lett.*, 1996, **251**, 365–371.
20 B. O. Roos and P.-A. Malmqvist, *Phys. Chem. Chem. Phys.*, 2004, **6**, 2919–2927.
21 L. F. Chibotaru and L. Ungur, *J. Chem. Phys.*, 2012, **137**, 064112–064122.
22 (*a*) L. F. Chibotaru, L. Ungur, C. Aronica, H. Elmoll, G. Pilet and D. Luneau, *J. Am. Chem. Soc.*, 2008, **130**, 12445–12455; (*b*) H. L. C. Feltham, R. Clérac, L. Ungur, V. Vieru, L. F. Chibotaru, A. K. Powell and S. Brooker, *Inorg. Chem.*, 2012, **51**, 10603–10612; (*c*) P.-H. Guo, J.-L. Liu, Z.-M. Zhang, L. Ungur, L. F. Chibotaru, J.-D. Leng, F.-S. Guo and M.-L. Tong, *Inorg. Chem.*, 2012, **51**, 1233–1235; (*d*) J.-L. Liu, J.-Y. Wu, G.-Z. Huang, Y.-C. Chen, J.-H. Jia, L. Ungur, L. F. Chibotaru, X.-M. Chen and M.-L. Tong, *Sci. Rep.*, 2015, **5**, 16621; (*e*) S. K. Langley, N. F. Chilton, L. Ungur, B. Moubaraki, L. F. Chibotaru and K. S. Murray, *Inorg. Chem.*, 2012, **51**, 11873–11881; (*f*) S. K. Langley, N. F. Chilton, B. Moubaraki and K. S. Murray, *Inorg. Chem. Front.*, 2015, **2**, 867–875; (*g*) S. K. Langley, L. Ungur, N. F. Chilton, B. Moubaraki, L. F. Chibotaru and K. S. Murray, *Inorg. Chem.*, 2014, **53**, 4303–4315; (*h*) S. K. Langley, N. F. Chilton, B. Moubaraki and K. S. Murray, *Chem. Commun.*, 2013, **49**, 6965–6967; (*i*) P. H. Lin, N. C. Smythe, S. I. Gorelsky, S. Maguire, N. J. Henson, I. Korobkov, B. L. Scott, J. C. Gordon, R. T. Baker and M. Murugesu, *J. Am. Chem. Soc.*, 2011, **133**, 15806–15809; (*j*) J.-L. Liu, J.-Y. Wu, Y.-C. Chen, V. Mereacre, A. K. Powell, L. Ungur, L. F. Chibotaru, X.-M. Chen and M.-L. Tong, *Angew. Chem., Int. Ed.*, 2014, **53**, 12966–12970; (*k*) V. S. Mironov, L. F. Chibotaru and A. Ceulemans, *J. Am. Chem. Soc.*, 2003, **125**, 9750–9760; (*l*) L. Ungur, W. Van den Heuvel and L. F. Chibotaru, *New J. Chem.*, 2009, **33**, 1224–1230; (*m*) K. R. Vignesh, S. K. Langley, K. S. Murray and G. Rajaraman, *Inorg. Chem.*, 2017, **56**, 2518–2532; (*n*) S. Xue, L. Ungur, Y.-N. Guo, J. Tang and L. F. Chibotaru, *Inorg. Chem.*, 2014, **53**, 12658–12663.
23 M. E. Lines, *J. Chem. Phys.*, 1971, **55**, 2977–2984.
24 L. F. Chibotaru and L. Ungur, *POLY_ANISO program*, University of Leuven, 2006.
25 (*a*) J. Cirera, E. Ruiz and S. Alvarez, *Chem. – Eur. J.*, 2006, **12**, 3162–3167; (*b*) M. Pinsky and D. Avnir, *Inorg. Chem.*, 1998, **37**, 5575–5582.
26 (*a*) Y.-S. Ding, Y.-Q. Zhai, R. Winpenny and Y.-Z. Zheng, *ChemRxiv*, 2018, DOI: 10.26434/chemrxiv.7083038; (*b*) T. Gupta and G. Rajaraman, *Eur. J. Inorg. Chem.*, 2018, **2018**, 3402–3412; (*c*) T. Gupta, G. Velmurugan, T. Rajeshkumar and G. Rajaraman, *J. Chem. Sci.*, 2016, **128**, 1615–1630; (*d*) K. R. Vignesh, D. I. Alexandropoulos, B. S. Dolinar and K. R. Dunbar, *Dalton Trans.*, 2019, **48**, 2872–2876.
27 N. F. Chilton, *CC-fit*, The Univesity of Manchester, UK, 2014, http://www.nfchilton.com/cc-fit.html.
28 D. Sertphon, K. S. Murray, W. Phonsri, J. Jover, E. Ruiz, S. G. Telfer, A. Alkas, P. Harding and D. J. Harding, *Dalton Trans.*, 2018, **47**, 859–867.
29 K. N. Shrivastava, *Phys. Status Solidi B*, 1983, **117**, 437–458.
30 Y.-X. Wang, W. Shi, H. Li, Y. Song, L. Fang, Y. Lan, A. K. Powell, W. Wernsdorfer, L. Ungur, L. F. Chibotaru, M. Shen and P. Cheng, *Chem. Sci.*, 2012, **3**, 3366–3370.
31 (*a*) P. Panissod and M. Drillon, in *Magnetism: Molecules to Materials IV*, ed. J. S. Miller and M. Drillon, Wiley-VCH Verlag GmbH & Co. KGaA, Weinheim, 2002, ch. 7, p. 235; (*b*) J.-D. Leng, J.-L. Liu, W.-Q. Lin, S. Gomez-Coca, D. Aravena, E. Ruiz and M.-L. Tong, *Chem. Commun.*, 2013, **49**, 9341–9343.
32 L. Ungur, S.-Y. Lin, J. Tang and L. F. Chibotaru, *Chem. Soc. Rev.*, 2014, **43**, 6894–6905.